Investigation of adhesion recovery phenomenon using a scaled roller-rig

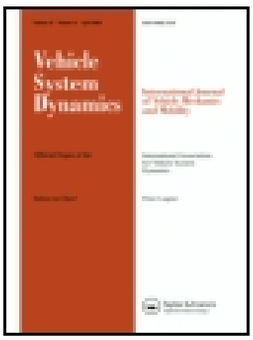

Taylor & Francis
Taylor & Francis Group

Vehicle System Dynamics
International Journal of Vehicle Mechanics and Mobility

ISSN: 0042-3114 (Print) 1744-5159 (Online) Journal homepage: https://www.tandfonline.com/loi/nvsd20

Investigation of adhesion recovery phenomenon using a scaled roller-rig

N. Bosso, M. Magelli & N. Zampieri

To cite this article: N. Bosso, M. Magelli & N. Zampieri (2019): Investigation of adhesion recovery phenomenon using a scaled roller-rig, Vehicle System Dynamics, DOI: 10.1080/00423114.2019.1677922

To link to this article: https://doi.org/10.1080/00423114.2019.1677922

VEHICLE SYSTEM DYNAMICS
https://doi.org/10.1080/00423114.2019.1677922

Investigation of adhesion recovery phenomenon using a scaled roller-rig

N. Bosso, M. Magelli and N. Zampieri

Department of Mechanical and Aereospace Engineering, Politecnico di Torino, Torino, Italy

ABSTRACT

When high creep values occur on a braked/trailing wheelset running on a contaminated track, changes in the friction conditions take place. In fact, the work of the friction forces gradually removes the contaminant from the wheel and rail surfaces. Therefore, lower levels of adhesion are present on the leading wheelsets, while better conditions are restored on the following ones. A deep understanding of this phenomenon is needed to develop new algorithms for WSP and antiskid systems, in order to maximise the tractive/braking performances of railway vehicles. The research group of the Politecnico di Torino has recently designed an innovative multi-axle roller-rig to investigate the adhesion recovery phenomenon. First, the paper briefly shows the configuration of the new roller-rig, then focus is given to the experimental results obtained from adhesion recovery tests performed on the test bench.

ARTICLE HISTORY
Received 26 June 2019
Revised 9 September 2019
Accepted 30 September 2019

KEYWORDS
Adhesion; adhesion recovery; roller-rig; wheel-rail contact; friction

List of Symbols

Latin Alphabet

d_w	Wheel diameter
d_R	Roller diameter
f	Adhesion Coefficient
F_x	Tangential load at the wheel-roller interface
$I_{w,yy}$	Polar inertia of the wheelset
N	Normal load at the wheel/roller interface
N_s	Suspension load
p_{FB}	Calliper pressure (f/b)
p_{SET}	Calliper pressure (set)
T_b	Braking torque
T_M	Torque produced by the motor

CONTACT N. Zampieri nicolo.zampieri@polito.it

Greek Alphabet

$\omega_{R,FB}$	Angular speed of the rollers (f/b)
$\omega_{R,SET}$	Angular speed of the rollers (set)
ω_w	Angular speed of the wheels
$\dot{\omega}_w$	Angular acceleration of the wheelset

Subscripts

b	Braking
FB	Feedback
i	Wheelset number ($i = 1 \div 4$)
j	Wheel number ($j = 1,2$)
R	Roller
s	Suspension
SET	Set
w	wheelset

1. Introduction

In railway transportation systems, the adhesion coefficient plays a fundamental role with regard to performances, punctuality and safety during both braking and traction manoeuvres.

Contact conditions can be seriously affected by contaminants lying on the track, which can cause a significant drop in the adhesion level. Water and oil introduce lubricated friction [1] instead of the typical dry friction conditions. Beagley et al. [2,3] made use of a laboratory device consisting of a disc rolling over a plate and showed that water can reduce the adhesion coefficient from $f = 0.6$ to $f = 0.3$, while oil is responsible for lower values ($f = 0.15$). Zhu et al. [4] used a mini traction machine (MTM) to investigate the dependency of Stribeck and adhesion curves on surface roughness, fluid temperature and normal contact pressure. A numerical contact model was developed based on the experimental results [5]. According to many authors, autumn leaves can cause the lowest values of the adhesion coefficient ($f = 0.07$–0.15) [6–8]. Experimental tests carried out by means of a twin-disc machine showed that an instant drop in the adhesion level can occur when leaves are added between the disc surfaces for both dry and wet contact conditions [9].

Sand is usually spread on the rails to restore dry contact adhesion for both wet and leaf-contaminated tracks, however sanding increases the wear rate of wheel and rail surfaces [10–13].

Engineered products, referred to as friction modifiers (FMs), are spread on the rails to keep adhesion at a constant optimum level in order to optimise the running behaviour of railway vehicles in terms of punctuality, wear rate, energy consumption, rolling contact fatigue (RCF) and noise [14–17]. Moreover, FMs modify the adhesion characteristic in order to obtain a monotonic dependency of adhesion with respect to creepage [14,17–19]. This allows to obtain a more regular traction effort. Modern

vehicles are equipped with mechatronic devices intended to properly manage the distribution of the braking (Wheel slide protection, or WSP, systems) [20–23] or tractive (Anti-skid systems) [24,25] effort among the wheels. Modelling degraded adhesion conditions is thus fundamental to develop new efficient contact algorithms [26] for these systems.

When a vehicle is running on a contaminated track, the friction forces developed by the leading wheelsets have a cleaning effect on the rails, so that dry adhesion conditions can be partially restored on the following wheels. This phenomenon can be referred to as *rail adhesion recovery*. Moreover, the friction forces cause the progressive removal of the contaminant layer which sticks to the wheel surface itself. The term *wheel adhesion recovery* can be used to describe this phenomenon. Since both phenomena are related to the work of the friction forces and are not easy to single out during normal railway operations, the simple expression *adhesion recovery* is used in the paper for the sake of clarity.

Figure 1(a,b) shows a four-axle vehicle running over a water-contaminated track, during a braking manoeuvre: when the leading wheelset faces the contaminant, the highest values of creepage are recorded. The contaminant is thus partially removed, and lower values of creepage are observed on the following wheelsets (*rail adhesion recovery*). Being this phenomenon not deeply known at present, the linear trend of the creepage in Figure 1(b) is just a conceptual scheme to better highlight the behaviour of the following wheelsets of the vehicle when a contaminant is lying on the track.

Voltr and Lata [27,28] investigated the *wheel adhesion recovery* by means of a full-scale single wheel roller-rig and carried out several tests for both low and high adhesion conditions. They showed that interrupting the low adhesion tests when the creepage value was less than 100% caused a hysteretic loop in the curves, linked to the cleaning effect. A similar result was observed by Zhang et al. using a full-scale roller-rig [29]. On the other hand, if

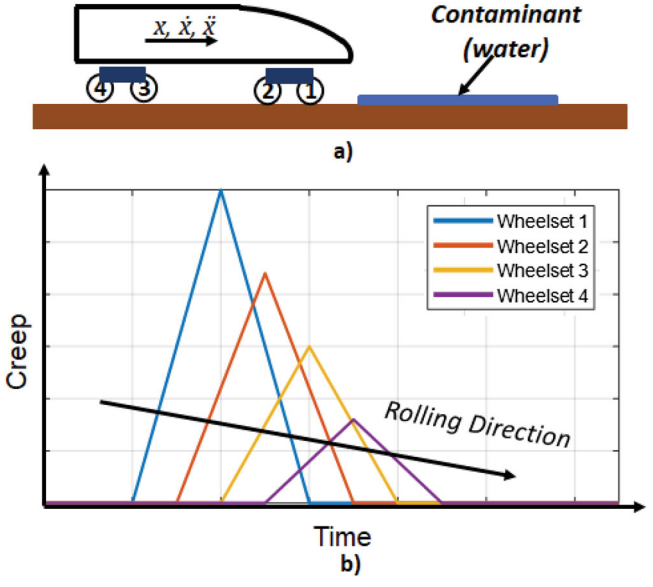

Figure 1. (a) Adhesion recovery scheme and (b) simplified creep time history.

creepage was allowed to reach higher values (up to 700% in traction conditions), a steady-state adhesion-decreasing trend could be observed, since the contaminant was completely removed. This behaviour was modelled by the authors admitting that the adhesion coefficient can vary from a lower to an upper curve: the latter is characterised by a higher value of the parameter μ_0 which appears in Polach's equations (see [30]). The variation $\Delta\mu_0$ can be calculated as a function of the dissipated energy at the interface. An energetical approach was followed also by Allotta et al. to develop a degraded adhesion model, implemented in a HIL architecture [31–33]. Adhesion curves shown by SNCF and UIC technical reports consider the *wheel adhesion recovery* too, since they consist of both an adhesion loss and an adhesion recovery course [34–36].

The *rail adhesion recovery* phenomenon is more difficult to study with respect to *wheel adhesion recovery*, since the mutual interaction of following wheels needs to be simulated. Bosso et al. [37] tried to use a single wheelset 1:5 scaled roller-rig [38], provided with a contamination system on the roller and a cleaning system on the wheel. The latter was intended to guarantee that at each revolution, a clean portion of the wheel faced a contaminated section of the roller, thus simulating the passage of multiple wheels. However, the inefficiencies of the cleaning system could lead to a difficult interpretation of the experimental results. To overcome these issues, the research group has recently designed an innovative multi-axle roller-rig, made up of four 1:5 scaled wheelsets running over the same pair of rollers [39,40].

The main goal of the paper is the evaluation of the wheel and rail adhesion recovery phenomena by means of the multi-axle roller-rig. The innovative architecture of the test bench allows to evaluate, in laboratory environment, the evolution of the friction conditions due to the actions of several wheelsets running on the same section of contaminated track. This aspect (i.e. the mutual influence of several wheelsets running on the same track), is the main novelty of this work. The experimental results demonstrate that the mutual influence among the wheelsets plays a fundamental role in the adhesion characteristic.

The first section of the paper deals with a brief description of the bench design and control and of the data acquisition strategy, while the second part focuses on the experimental results obtained from both wheel and rail adhesion recovery tests performed on the roller-rig.

2. Experimental setup and device

2.1. The multi-axle roller-rig and the data acquisition strategy

The multi-axle roller-rig (see Figure 2) is a 1:5 scaled test rig which follows the similitude model proposed by Jaschinski [41].

The test bench consists of four wheelsets (1) rolling over the same pair of rollers (2). Each wheel, with a diameter $d_w = 0.184$ m, is made up of a hub and a rim, which reproduces the 1:5 scaled S1002 profile. The surfaces of the rollers ($d_R = 0.368$ m) replicate a 1:5 scaled UIC60 profile, canted 1:20. The two rollers are rigidly connected through a mechanical joint and they are powered using a 6 poles brushless AC Motor (ACM BRL 220 6), controlled by a Control Techniques™ UNIDRIVE SP4402 drive. The longitudinal position of each wheelset can be independently adjusted: the connections to the main frame (3) in both longitudinal and lateral directions can be considered as rigid. On the other hand, each

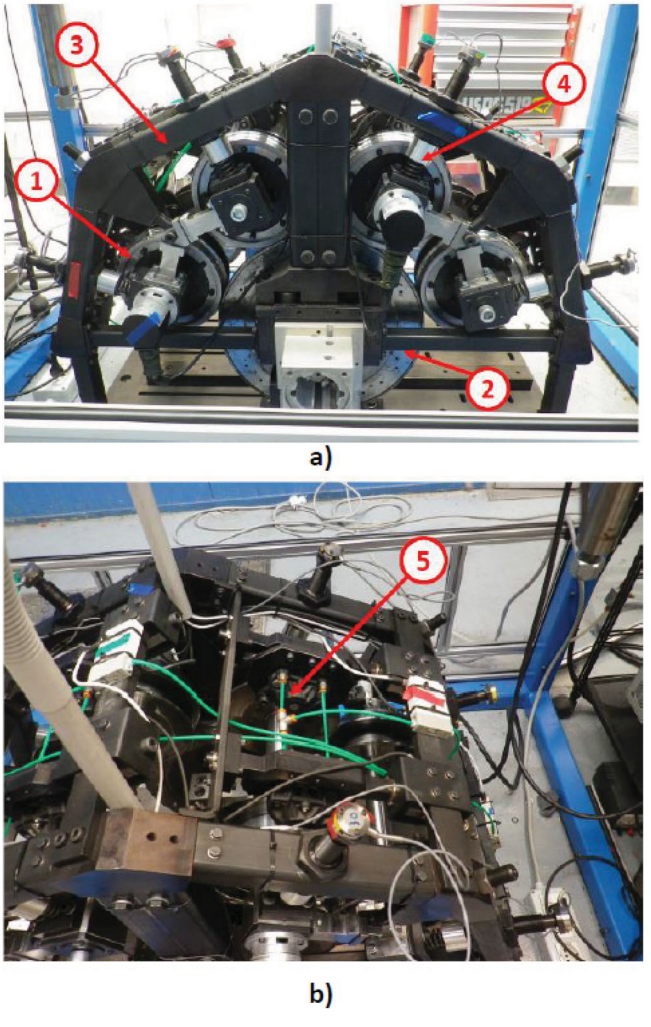

Figure 2. (a) Multi-axle roller-rig: front view and (b) detail of the braking system.

axle-box is provided with a spring suspension system (4), which allows to simulate different values of the normal load acting on the wheel-roller interface. All the adhesion curves shown in the paper have been obtained with a normal load of 80 kg, which corresponds to 10 ton per axle on a real vehicle.

Each wheelset is equipped with a pneumatic braking system (5) consisting of two brake discs and two callipers (Brembo P32G), in order to independently control the resistant torque on the wheelsets. The brushless motor is set to servo-mode and both speed and torque control can be performed.

To obtain adhesion curves, the bench is equipped with proper instrumentation, which is managed by an industrial PC (NI PXIe-8330), housed in a NI PXIe-1050 chassis.

The speeds of the four wheelsets can be obtained by means of four ELAP REM470–1024-8/24-R-10-PP2 incremental single-ended encoders (1024 pulses per revolution): the signals are acquired thanks to a NI PXIe-6612 digital I/O module.

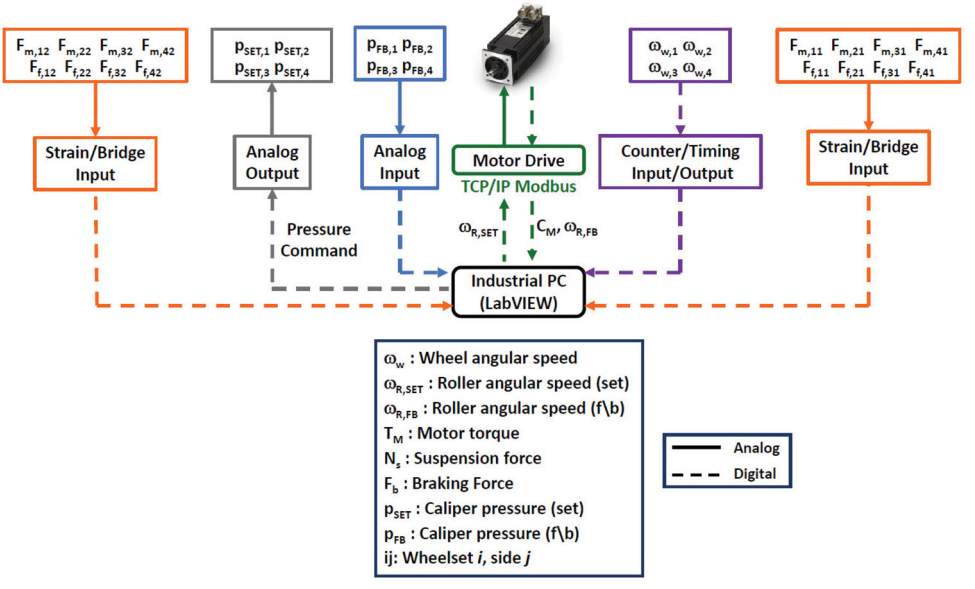

Figure 3. Data acquisition and test bench control strategy (scheme).

The normal load imposed by the suspension system mounted on each axle-box is measured by eight load button cells (FUTEK LLB 400 FSH 00877) with a maximum load of 1000 lb (454 kg) and a resolution equal to 0.5 lb (0.27 kg). The tangential load due to the braking effort on each calliper-disc pair is measured through eight S-beam load cells (FUTEK LSB 302 FSH 02089), characterised by a maximum load of 300 lb (136.2 kg) and a resolution of 0.15 lb (0.068 kg). The signals of all the load cells are acquired by using two 8-channel strain bridge input modules (NI PXIe-4330): more in detail, each module manages the signals coming from the four button cells and the four S-beam cells mounted on the same side of the rig.

The pressure acting on the callipers of each wheelset can be regulated thanks to four electro-pneumatic regulators SMC ITV005-3BS in the range 0–9 bar: the valves also provide the measurement of the feedback pressure. The pressure set signals are managed by an analog output NI USB-9263 module, while the feedback signals are acquired thanks to an analog input NI USB-9239 module.

The control of the bench and the acquisition of all the signals measured by the transducers is performed using a LabVIEW VI. The industrial PC can communicate with the motor drive through the TCP\IP Modbus protocol, so that the desired speed of the rollers can be set, and the feedback motor speed and torque can be registered during the tests. A schematic view of the data acquisition strategy and of the control of the roller-rig is shown in Figure 3.

The LabVIEW VI (see Figure 4) comprises 3 while loops:

(1) Loop 1 is intended to acquire all the data measured by the sensors installed on the bench, i.e. the angular position of the wheelsets, the normal and braking forces and the pressure acting on each braking system. Moreover, the communication between the industrial PC and the motor drive is established and the motor speed and torque

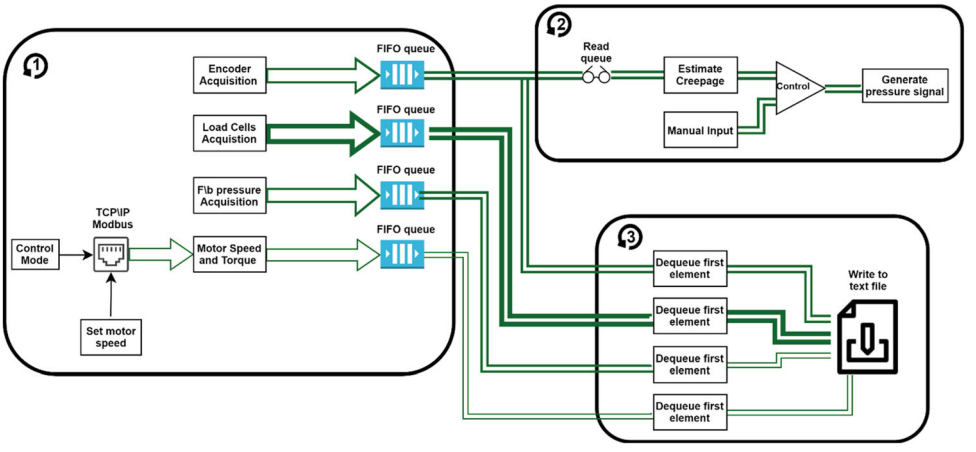

Figure 4. Block diagram of LabVIEW VI.

are registered. All the signals acquired in this loop are stored in queues, so that the acquisition and saving loops can run at different rates.

(2) Loop 2 allows to set a pressure signal to slow down each axle independently: the command can be either manual or be a function of the actual creep, estimated from the encoder measurements.

(3) Loop 3 removes the first element in each queue and saves data in a *text* file.

The experimental setup of the roller-rig has already been performed and described in [40], however the original LabVIEW VI has been improved using queues as shown in Figure 4 in order to increase the sampling frequency during the experimental tests. In fact, if the sampling rate is not high enough, all the original data acquired belongs either to the linear course of the adhesion characteristic or to the full sliding condition, when the wheel is locked. This is caused by the very quick variation of the creep value in the unstable part of the adhesion characteristic.

The new LabVIEW VI guarantees a sampling rate equal to 1 kHz, so that a higher number of points in the incipient locking phase can be recorded. The benefit of using queues is highlighted in Figure 5, which shows the original adhesion curves for wheelset 2 obtained with the old and the new LabVIEW VI: similar results are also valid for the other axles.

2.2. Repeatability of tests

The preliminary adhesion curves presented in [40] were obtained by braking the wheelsets with a pressure ramp characterised by a gradient m equal to 0.96 bar/s: the calliper pressure was released when the wheel locking was detected. However, before executing the adhesion recovery tests, adhesion curves were acquired by braking wheelset 1 with three different values of the slope m (see Figure 6(a)), to ensure that the experimental results would not be affected by the pressure ramp. A good repeatability of the adhesion curves for all the ramps can be observed in Figure 6(b).

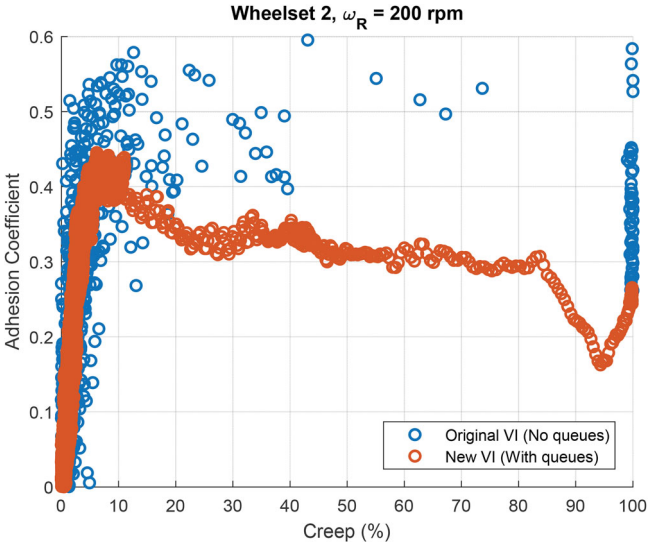

Figure 5. Comparison between old and new LabVIEW VI (Wheelset 2, $\omega_R = 200$ rpm).

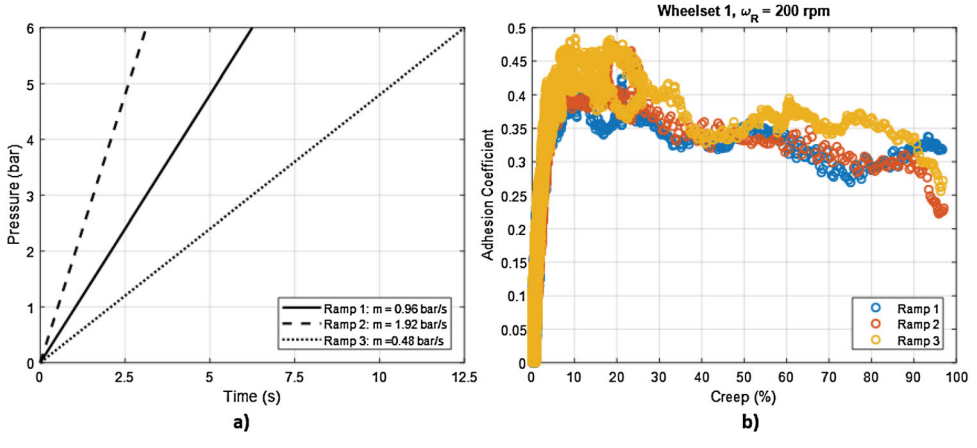

Figure 6. (a) Tested pressure ramps and (b) repeatability of adhesion curves.

The adhesion coefficient for each wheelset (f_i) is calculated with Equation 1 as the ratio between the longitudinal ($F_{x,i}$) and normal (N_i) forces acting on the wheel-roller interface:

$$f_i = \frac{F_{x,i}}{N_i} \tag{1}$$

The longitudinal force $F_{x,i}$ can be obtained with an equilibrium of momentum for the braked wheelset (see Figure 7) using Equation 2:

$$F_{x,i} = \frac{2}{d_w}(T_{b,i} - I_{w,yy}\dot{\omega}_{w,i}) \tag{2}$$

where:

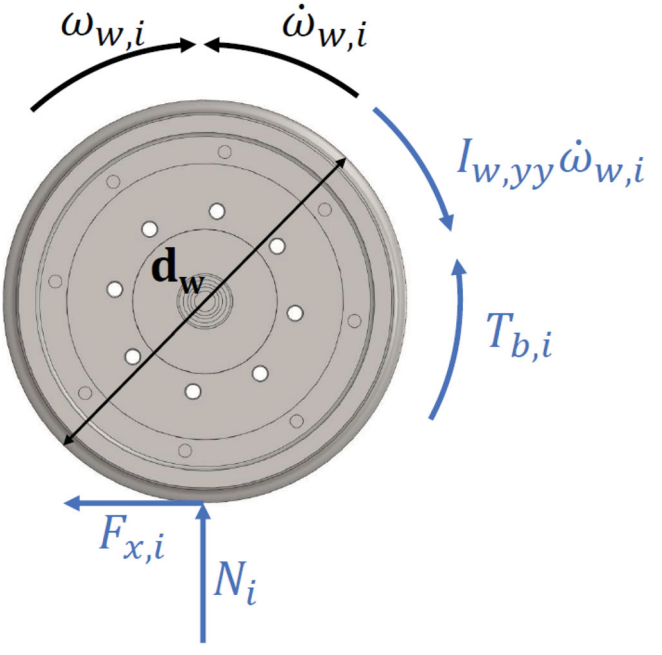

Figure 7. Equilibrium of momentum of the braked wheelset.

- d_w is the wheel diameter (0.184 mm);
- $T_{b,i}$ is the braking torque acting on braked wheelset, which is derived from the signals of the S-beam load cells;
- $I_{w,yy}$ is the polar momentum of inertia of the wheelset, estimated from the CAD model of the test bench and equal to 0.051 kg·m^2;
- $\dot{\omega}_{w,i}$ indicates the angular acceleration of the i wheelset, which can be calculated with a numerical differentiation of the encoder measurements.

The inertial term in Equation 2 is typically neglected when both the wheels and the rollers are powered, and their speed is controlled so that a quasi-steady-state condition is achieved during the tests: this is the typical situation for twin-disc machines [11,12,42,43]. However, in the multi-axle roller-rig only the rollers are powered, whereas the wheelsets are braked with a pneumatic system. The wheel locking phenomenon is clearly unstable and thus the angular deceleration of the braked wheelset cannot be neglected. Figure 8 shows the differences in the adhesion curves calculated on the same set of experimental data considering and neglecting the angular deceleration: when the inertial term is not taken into account, the adhesion coefficient is overestimated as required by Equation 2.

As previously mentioned, the brushless motor, powering the rollers, can be controlled both in speed and torque. Therefore, two series of adhesion tests were conducted braking one wheelset at a time with a slope of the pressure ramp equal to 0.96 bar/s (see ramp 1 in Figure 6 (a)) and setting the speed of the rollers to 200 rpm ($\approx$ 30 km/h for a real vehicle). In the first set of tests the drive controlled the speed of the motors, whereas in the second series, a torque control was performed.

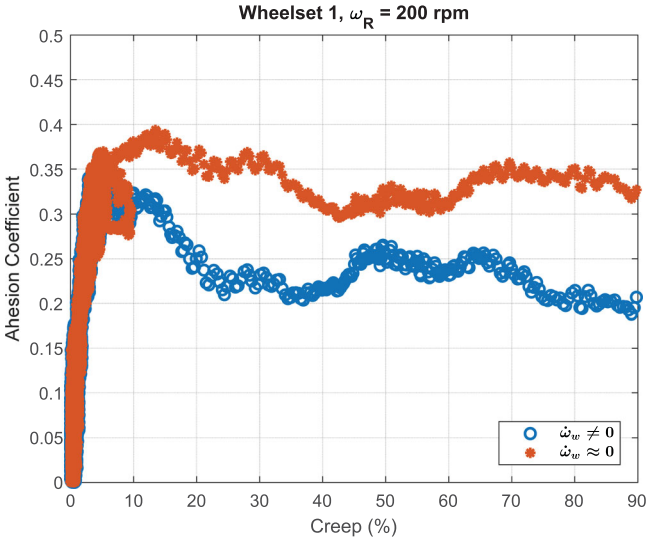

Figure 8. Influence of the inertial term on adhesion curves.

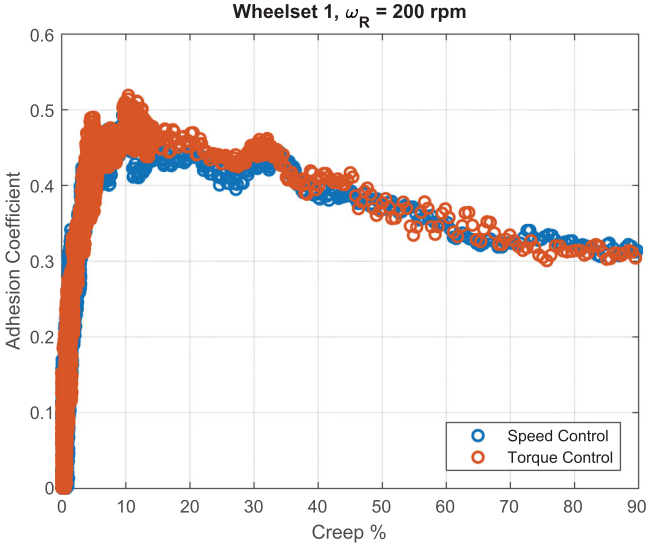

Figure 9. Influence of control mode on adhesion curves.

A good agreement between the torque and speed control was obtained. Figure 9 shows the adhesion curves obtained on wheelset 1 considering the two control modes. Therefore, it can be concluded that the results are slightly affected by the pressure ramp and by the motor control strategy. However, the experimental activity has highlighted that the torque control guarantees a stable behaviour of the motor in a wider range of speed with respect to the speed control. Therefore, the adhesion recovery tests shown in the following section were performed in torque control mode.

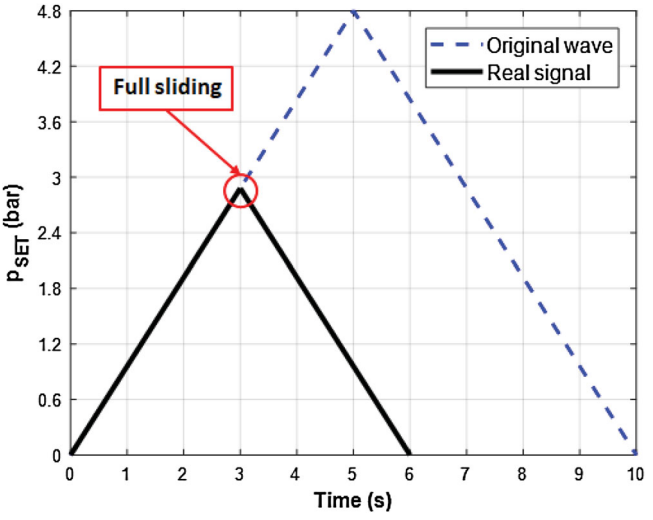

Figure 10. Pressure signal for wheel adhesion recovery tests.

3. Results and discussion

This section deals with the experimental tests performed on the bench to investigate both the wheel and the rail adhesion recovery phenomena. The *wheel adhesion recovery* phenomenon was investigated braking one single axle, while the *rail adhesion recovery* test was carried out braking all the wheelsets at the same time.

3.1. Wheel adhesion recovery tests

The *wheel adhesion recovery* tests were performed by braking the wheelset 3 with a triangular wave pressure signal, composed by four lines with a slope equal to ± 0.96 bar/s. However, when full sliding conditions were detected, the triangular wave signal was interrupted and the calliper pressure was gradually released with the same gradient. Figure 10 shows half of the original triangular wave signal, with an amplitude of 4.8 bar and a frequency of 0.05 Hz (blue dashed curve), and the real signal used to control to the valve (black curve), in the hypothesis that full sliding is reached when the pressure is equal to 2.8 bar.

The tests investigated both dry and wet contact conditions. Before each wet test, the surfaces of the rollers were contaminated with water. Figure 11 shows a schematic view of the *wheel adhesion recovery* test performed on wheelset 3 in wet conditions (see the blue layer over the roller surface). The same strategy is applied for dry tests, but no water layer is present on the surfaces.

The adhesion curve obtained in the dry test with the roller speed set to 100 rpm is presented in Figure 12. Since there is no contamination on the wheel-roller interface, the forward (i.e. increasing creep) and backward (i.e. decreasing creep) cycle curves are extremely similar to each other, and no significant hysteretic loop can be observed.

The *wheel adhesion recovery* tests in wet conditions were executed for three different values of the roller speed: 100, 200 and 300 rpm (i.e. $\approx$ 15, 30 and 45 km/h for a real vehicle). Low speed values are considered in order to limit the damage to the wheel and roller

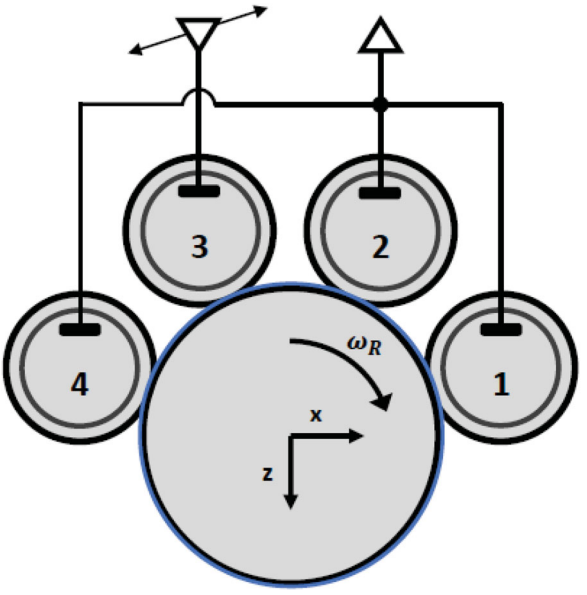

Figure 11. Scheme of adhesion recovery test for wet conditions.

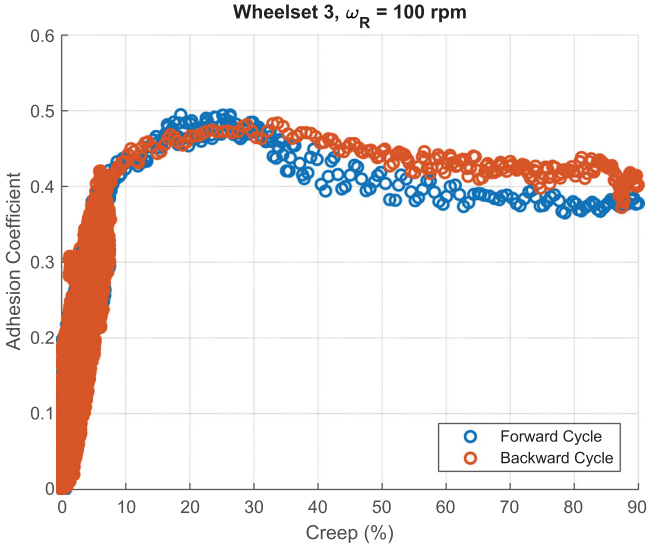

Figure 12. Wheel adhesion recovery test ($\omega_R = 100$ rpm, dry conditions).

surfaces. The adhesion characteristics are shown in Figure 13(a–c). With respect to dry adhesion conditions shown in Figure 12, a significant drop in the adhesion level can be observed for all speeds, because of the contaminant lying at the interface.

Moreover, the comparison of the three characteristics shows a strong dependency on the roller speed. In fact, when the roller rotates at 100 rpm, a slender hysteretic loop can be observed, while in the 200 rpm test the loop is wider. Finally, the 300 rpm test shows a noticeable adhesion recovery in the forward course for a creep value of approximately 45%,

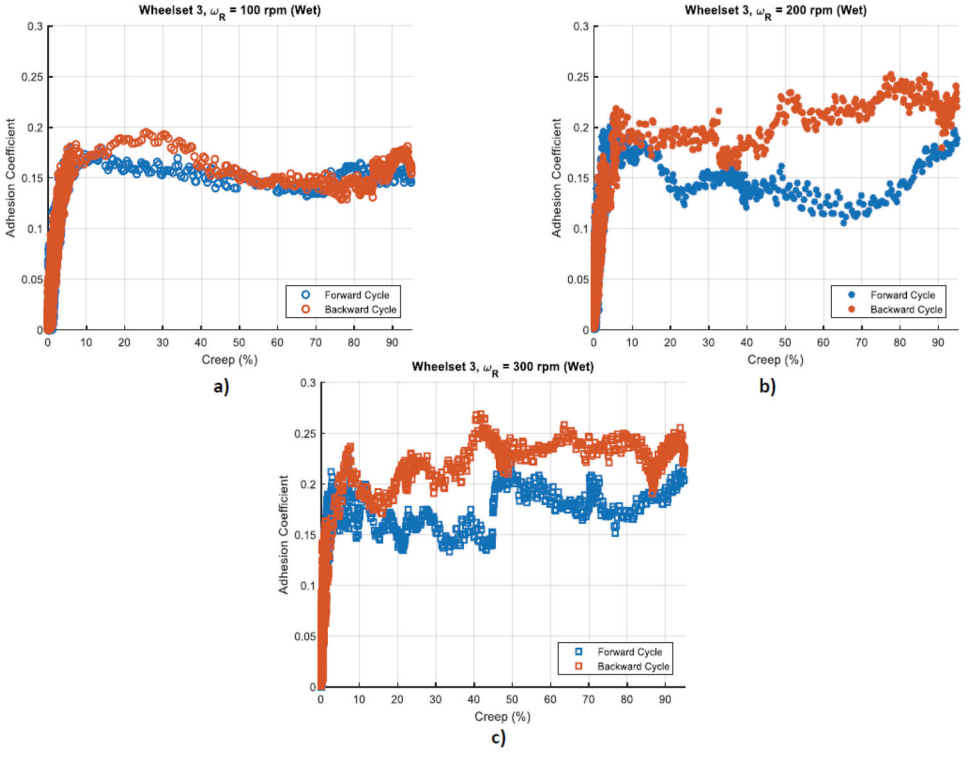

Figure 13. (a) Wheel adhesion recovery test (wet contact conditions) for $\omega_R = 100$, (b) 200 and (c) 300 rpm.

and higher values of adhesion in the backward cycle. These differences could be related to changes in the wheel-roller interface temperature to varying the roller speed.

However, this hypothesis cannot be confirmed at the current state of work since the bench is not equipped with sensors able to estimate the temperature on the contact patch. Moreover, another possible reason to explain this distinction could coincide with the strategy of application of the contaminant, which does not allow to control the quantity of water spread onto the surfaces.

3.2. Rail adhesion recovery tests

The mutual interaction among the four wheelsets on a contaminated track (i.e. the *rail adhesion recovery* phenomenon) was investigated by braking all the axles with a constant pressure equal to 1.5 bar, so as to guarantee full adhesion conditions when the surfaces of the rollers are clean. The speed of the motor was set to 390 rpm ($\approx$ 60 km/h for a real vehicle) and during the test, some wet sheets were pressed against the rotating rollers to contaminate the interface (see Figure 14).

Figure 15 shows the creepage time history: three peaks in the creep value can be observed for all the wheelsets, which are related to three separate applications of the contaminant. For all the applications, wheelset 4 reaches the highest values in creepage, while the lowest can be observed on wheelset 1. This is consistent with the clockwise direction

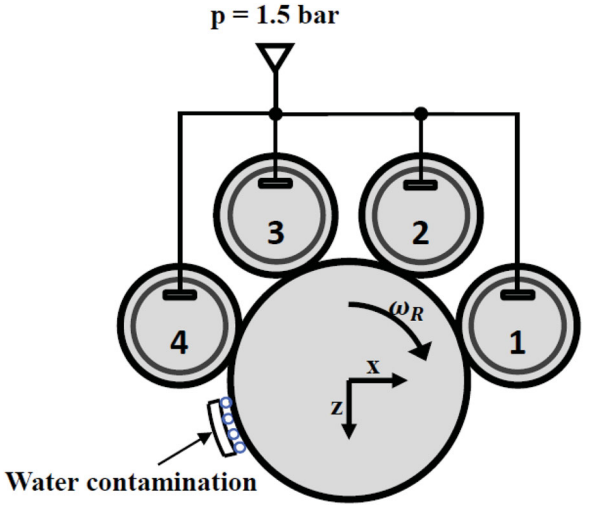

Figure 14. Schematic representation of rail adhesion recovery test.

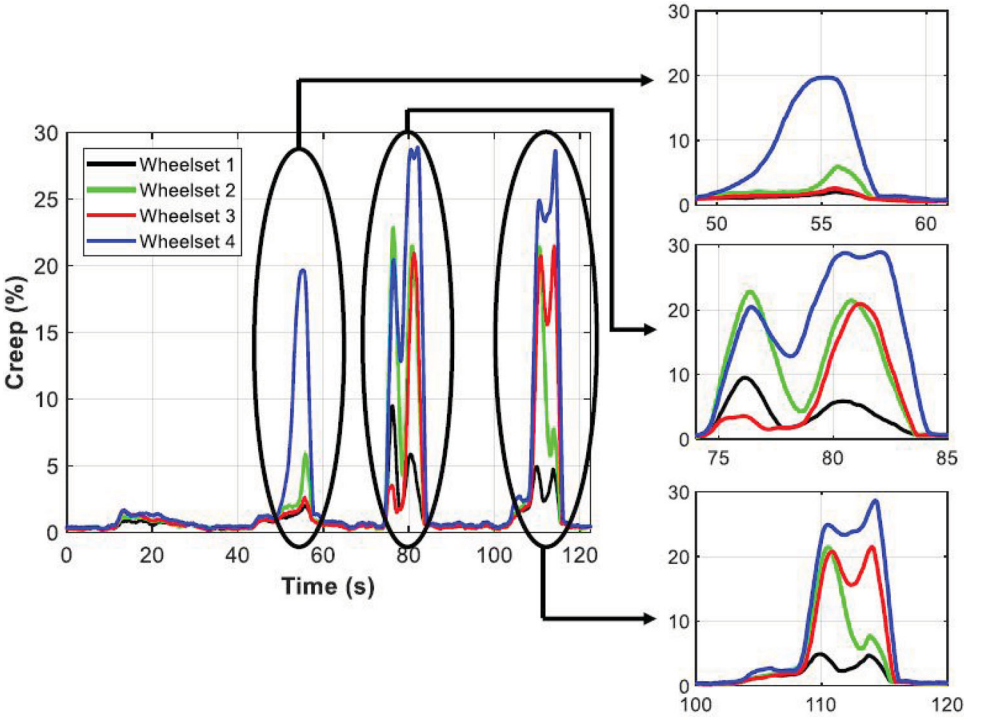

Figure 15. Creep time history in rail adhesion recovery test.

of rotation of the rollers as shown in Figure 14. Moreover, the increase in creepage can always be first registered on wheelset 4, which is the first one to face the wet section of the roller. Finally, after each contamination, all the axles reach their original creepage values, which means that the contaminant has totally been removed by the work of the friction

forces. Differences among the zooms in Figure 15 can be related to the test strategy, which currently does not allow to control and adjust the quantity of contaminant deposed at the interface. Another explanation could be a variation in the adhesion conditions of the four wheelsets. At the same time, vibrations and backlashes in the threaded connection of the suspension systems could create discrepancies in the compensation of the wheel/roller normal load.

However, the experimental results are extremely encouraging since the test bench proved to be a suitable laboratory device for the investigation of the *rail adhesion recovery*.

Conclusions

The paper concerns low adhesion conditions in railway transportation systems. When a braked/trailing wheelset reaches high values of creepage while running over a contaminated track, the lost energy due to the friction forces causes a gradual removal of the contaminant. Therefore, higher adhesion levels can be observed both on the braked/trailing wheelset (*wheel adhesion recovery*) and on the following axles (*rail adhesion recovery*), because of the cleaning of the wheel and rail surfaces. The *wheel adhesion recovery* has been investigated by many authors and numerical models have been proposed to describe the phenomenon. A laboratory investigation of the *rail adhesion recovery* is harder to perform since the mutual interaction among the wheelsets of a railway vehicle must be simulated. The research group of the Politecnico di Torino has thus realised an innovative 1:5 scaled roller-rig made up of four wheelsets rolling over the same pair of rollers. The bench is intended to study both *wheel* and *rail adhesion recovery* phenomena during braking manoeuvres. The configuration of the multi-axle roller-rig is such that the rollers are powered with a brushless motor, while a resistant torque is independently generated on each wheelset by means of a pneumatic braking system.

A good repeatability of the adhesion curves obtained to varying the command pressure ramp has been shown in the first part of the article, as well as a good agreement in the results acquired with speed and torque control of the motor. Moreover, it has been demonstrated that the angular deceleration of the braked wheelset cannot be neglected since the locking wheel phenomenon is unstable and extremely quick.

By braking one axle at a time, the *wheel adhesion recovery* phenomenon can be investigated. In the dry contact test, no significant hysteretic loop is noticed, since there is no contaminant to remove. On the other hand, a recovery in the adhesion level can be observed for all the tested values of the roller speed in the wet tests. However, this phenomenon has proved to be strongly dependant on the roller speed. This behaviour can be related to changes in the temperature at the wheel-roller interface, though this hypothesis must be confirmed in future works by equipping the test rig with proper sensors.

The paper also presents a *rail adhesion recovery* test. The results are in line with the expectations since the first axle to face the contaminant shows the highest values of creepage, while the last axle is the least significantly affected by the water spread onto the surfaces of the rollers.

The tests performed during the experimental activity have demonstrated that the multi-axle roller-rig is a suitable solution to study the adhesion recovery phenomena during railway braking operations. Further work is needed to investigate the influence of the roller speed, the normal load and the kind of contaminant on the adhesion curves. Future

activities will deal with the numerical modelling of the adhesion characteristics obtained during the tests. Moreover, the bench can be provided with digital valves to study and validate new WSP algorithms which can improve the braking performances of railway vehicles.

Conflict of interests

On behalf of all authors, the corresponding author states that there is no conflict of interest.

Disclosure statement

No potential conflict of interest was reported by the authors.

ORCID

N. Bosso http://orcid.org/0000-0002-5433-6365
N. Zampieri http://orcid.org/0000-0002-9197-1966

References

[1] Stribeck R. Die wesentlichen eigenschaften der gleit-und rollenlager. Zeitschrift des Vereines Deutscher Ingenieure. 1902;46:1341–1348. 1432-1438, 1463-1470.
[2] Beagley TM, McEwen IJ, Pritchard C. Wheel/rail adhesion—boundary lubrication by oily fluids. Wear. 1975;31(1):77–88.
[3] Beagley TM, Pritchard C. Wheel/rail adhesion — the overriding influence of water. Wear. 1975;35(2):299–313.
[4] Zhu Y, Olofsson U, Persson K. Investigation of factors influencing wheel-rail adhesion using a mini-traction machine. Wear. 2012;292-293:218–231.
[5] Zhu Y, Olofsson U, Söderberg A. Adhesion modeling in the wheel-rail contact under dry and lubricated conditions using measured 3D surfaces. Tribol Int. 2013;61:1–10.
[6] Moore DF. Chapter 14 - transportation and Locomotion. Prin Appl Tribol. 1975: 302–330, Pergamon.
[7] Fulford C. Review of low adhesion research. Report published by the Rail Safety and Standards Board, UK; 2004.
[8] Olofsson U. Adhesion and friction modification. In: Lewis R, Olofsson U, editors. Wheel-rail interface handbook. Chapter 17. Boca Raton: CRC Press; 2009. p. 510–527.
[9] Gallardo-Hernandez EA, Lewis R. Twin disc assessment of wheel/rail adhesion. Wear. 2008;265(9-10):1309–1316.
[10] Lewis R, Dwyer-Joyce RS. Wear at the wheel/rail interface when sanding is used to increase adhesion. Proc Inst Mech Eng Part F: J Rail Rapid Transit. 2006;220(1):29–41.
[11] Omasta M, Machatka M, Smejkal D, et al. Influence of sanding parameters on adhesion recovery in contaminated wheel-rail contact. Wear. 2015;322-323:218–225.
[12] Arias-Cuevas O, Li Z, Lewis R. A laboratory investigation on the influence of the particle size and slip during sanding on the adhesion and wear in the wheel-rail contact. Wear. 2011;271 (1-2):14–24.
[13] Arias-Cuevas O, Li Z, Lewis R. Investigating the lubricity and electrical insulation caused by sanding in dry wheel-rail contacts. Tribol Lett. 2010;37(3):623–635.
[14] Kalousek J, Magel E. Modifying and managing friction. Railw Track Struct. 1997;93(5): 31–X4.
[15] Arias-Cuevas O, Li Z, Lewis R, et al. Rolling-sliding laboratory tests of friction modifiers in dry and wet wheel-rail contacts. Wear. 2010;268(3-4):543–551.
[16] Li Z, Arias-Cuevas O, Lewis R, et al. Rolling-sliding laboratory tests of friction modifiers in leaf contaminated wheel-rail contacts. Tribol Lett. 2009;33(2):97–109.

[17] Galas R, Omasta M, Krupka I, et al. Laboratory investigation of ability of oil-based friction modifiers to control adhesion at wheel-rail interface. Wear. 2016;368-369:230–238.
[18] Matsumoto A, Sato Y, Ono H, et al. Creep force characteristics between rail and wheel on scaled model. Wear. 2002;253(1-2):199–203.
[19] Harmon M, Lewis R. Review of top of rail friction modifier tribology. Tribol Mater, Surf Interface. 2016;10(3):150–162.
[20] Nakazawa SI, Hijikata D. Wheel slide protection system by the use of the tangential force in the macro slip area. Quarterly Report of RTRI (Railway Technical Research Institute). 2017;58(3):196–203.
[21] Barna G. Diagnosis of Wheel Slide Protection Systems for rail vehicles. 2012 17th International Conference on Methods & Models in Automation & Robotics (MMAR), pp. 331–336.
[22] Stützle T, Viereck U, Stribersky A, et al. Creepage control for use in wheelslide protection systems. IFAC Proceedings Volumes (IFAC-PapersOnline). 2006;39:597–602.
[23] Bosso N, Gugliotta A, Zampieri N. Design and testing of an innovative monitoring system for railway vehicles. Proc Inst Mech Eng, Part F: J Rail Rapid Transit. 2018;232(2):445–460.
[24] Kondo K. Anti-slip control technologies for the railway vehicle traction. 2012 IEEE Vehicle Power and Propulsion Conference, VPPC 2012; 2012. pp. 1306–1311.
[25] Pichlík P, Zdenek J. Overview of slip control methods used in locomotives. Trans Electr Eng. 2014;2:38–43.
[26] Bosso N, Gugliotta A, Zampieri N. RTCONTACT: an efficient wheel-rail contact algorithm for real-time dynamic simulations; 2012.
[27] Voltr P, Lata M. Transient wheel–rail adhesion characteristics under the cleaning effect of sliding. Veh Syst Dyn. 2015;53(5):605–618.
[28] Voltr P, Lata M, Černý O. Measuring of wheel–rail adhesion characteristics at a test stand. Eng Mech. 2012;181:1–11.
[29] Zhang W, Chen J, Wu X, et al. Wheel/rail adhesion and analysis by using full scale roller rig. Wear. 2002;253(1-2):82–88.
[30] Polach O. Creep forces in simulations of traction vehicles running on adhesion limit. Wear. 2005;258(7-8):992–1000.
[31] Allotta B, Meli E, Ridolfi A, et al. Development of an innovative wheel-rail contact model for the analysis of degraded adhesion in railway systems. Tribol Int. 2014;69:128–140.
[32] Allotta B, Conti R, Meli E, et al. Study of High-Speed Train Dynamics under Degraded Adhesion Conditions: an Innovative HIL Architecture for Full-Scale Roller-Rigs; 2014.
[33] Allotta B, Conti R, Meli E, et al. Development of a full-scale roller-rig to test high speed trains under degraded adhesion conditions. MESA 2014 - 10th IEEE/ASME International Conference on Mechatronic and Embedded Systems and Applications, Conference Proceedings, 2014.
[34] Adhesion during braking, and anti-skid devices. *Office for Research and Experiments of the International Union of Railways*; 1985.
[35] Boiteux M. Le probleme de l'adherence en freinage. Revue generale des chemins de fer. 1986;2:59–72.
[36] Boiteux M, Cadier M, Kling J, et al. Adherence en freinage et anti-enrayeurs. *Document technique DT257 (B164), Office de Recherches et d'Essays de L'Union Internationale des Chemins de fer*; 1992.
[37] Bosso N, Gugliotta A, Zampieri N. Strategies to simulate wheel-rail adhesion in degraded conditions using a roller-rig. Veh Syst Dyn. 2015;53(5):619–634.
[38] Bosso N, Soma A, Gugliotta A. Introduction of a wheel-rail and wheel-roller contact model for independent wheels in a multibody code. pp. 151–159.
[39] Bosso N, Gugliotta A, Zampieri N. A test rig for multi-wheelset adhesion experiments. Civil-Comp Proc. 2016;110.
[40] Bosso N, Gugliotta A, Magelli M, et al. Experimental setup of an innovative multi-axle roller rig for the investigation of the adhesion recovery phenomenon. Experimental Techniques; 2019.
[41] Jaschinski A. On the application of similarity laws to a scaled railway bogie model; 1991.

[42] Fletcher DI, Lewis S. Creep curve measurement to support wear and adhesion modelling, using a continuously variable creep twin disc machine. Wear. 2013;298-299(1):57–65.
[43] Wang WJ, Liu TF, Wang HY, et al. Influence of friction modifiers on improving adhesion and surface damage of wheel/rail under low adhesion conditions. Tribol Int. 2014;75:16–23.